Intercomparison of a correlated-photon-based method to measure detector quantum efficiency

Alan Migdall, Stefania Castelletto, Ivo Pietro Degiovanni, and Maria Luisa Rastello

We report on the absolute calibration of photodetector quantum efficiency by using correlated photon sources, performed independently at two laboratories, the National Institute of Standards and Technology and the Istituto Elettrotecnico Nazionale (IEN). The goal is to use an interlaboratory comparison to demonstrate the inherent absoluteness of the photon correlation technique by showing its independence from the particular experimental setup. We find that detector nonuniformity limited this comparison rather than uncertainty inherent in the method itself. The ultimate goal of these investigations is development of a robust measurement protocol that allows the uncertainties of individual measurements to be determined experimentally and verified operationally. Furthermore, to demonstrate the generality of the procedure, the IEN measurement setup was also used to calibrate a fiber-coupled avalanche photodiode module. Uncertainties are evaluated for the detector both with and without fiber coupling and differences are discussed. The current IEN setup using a thinner and higher transmittance nonlinear crystal for the generation of correlated photons shows a significant improvement in overall accuracy with respect to previously reported results from IEN [Metrologia **32**, 501–503 (1996)]. © 2002 Optical Society of America

OCIS codes: 030.5630, 040.5570, 120.3940, 120.4800, 120.5630.

1. Introduction

Recently a technique based on correlated photons obtained through parametric downconversion (PDC) has been studied for the absolute calibration of photon counters. The interest in this technique is establishment of inherently absolute measurements at very low light levels, i.e., in the photon-counting regime. This technique has proved successful for the absolute calibration of photomultipliers and avalanche photodiodes (APDs).[1–7] Although reports of this method have so far consisted of demonstrations and feasibility studies, much less emphasis has been given to systematic studies of uncertainty and independent verifications of that uncertainty. Without such efforts the impressive potential of this method will not be fully realized as a true metrological technique that can be used conveniently and with confi-

dence. The goal of this research is to provide some of this missing framework.

In the PDC process a pump field with angular frequency ω_p generates, by interaction with a $\chi^{(2)}$ nonlinear crystal, correlated pairs of signal and idler photons under the constraints of conservation of energy and wave-vector momentum:

$$\omega_p = \omega_s + \omega_i, \qquad \mathbf{k}_p = \mathbf{k}_s + \mathbf{k}_i, \qquad (1)$$

where ω_s and ω_i are signal and idler frequencies and $\mathbf{k}_p$, $\mathbf{k}_s$, and $\mathbf{k}_i$ are pump, signal, and idler wave vectors, respectively.

These conservation rules lead to pairs of photons that are strongly correlated both spatially and temporally. Using these rules with available crystals, one can produce signal and idler pairs that are emitted noncollinearly with the pump, allowing for easy optical discrimination and making these photon pairs useful for measuring the quantum efficiency of photodetectors operating in the photon-counting regime.[1–6,8]

When two correlated PDC emission channels corresponding to signal and idler photon propagation directions are appropriately selected, the detection of one photon of a PDC pair guarantees with certainty the presence of the second photon along the correlated direction. Selecting these two channels and di-

A. Migdall is with the Optical Technology Division of the National Institute of Standards and Technology, 100 Bureau Drive, Stop 8441, Gaithersburg, Maryland 20899-8441. S. Castelletto (castelle@ien.it), I. P. Degiovanni, and M. L. Rastello are with the Istituto Elettrotecnico Nazionale G. Ferraris, Strada delle Cacce 91 10135, Turin, Italy.
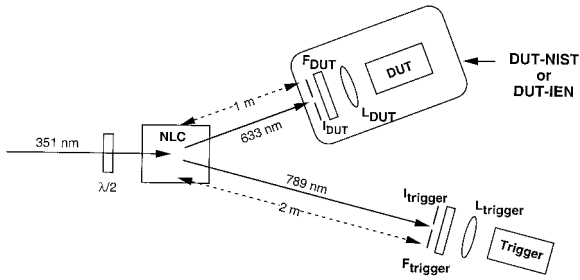
Fig. 1. Experimental setup for absolute quantum efficiency measurement comparison with correlated photons at 632.8 nm (DUT) and 789 nm (trigger): Ar^+, pump laser at 351 nm, F_{DUT}, $F_{trigger}$, interference filters at 632.8 and 789 nm, respectively. Irises I_{DUT} and $I_{trigger}$ are set according to procedure. DUT was in turn NIST SPCM-AQ-231 and IEN SPCM-AQ-152. The box around the DUT and its optics indicates that is considered as a unit.

recting them to two photon counters (A and B), we give the mean count rates at both channels (N_A, N_B) and in coincidence N_C, respectively, by

$$N_A = \eta_A N, \qquad N_B = \eta_B N, \qquad (2)$$

$$N_C = \eta_A \eta_B N, \qquad (3)$$

where η_A and η_B denote the counting efficiency of two photodetectors, A and B, respectively, and N is the rate of correlated pair production. Thus the quantum efficiencies are found directly:

$$\eta_A = \frac{N_C}{N_B}, \qquad \eta_B = \frac{N_C}{N_A}. \qquad (4)$$

Because in practice[7,9] it is difficult to arrange exactly that each detector sees only photons correlated to the other, we have to dedicate the channels to particular aims. One detector is the detector-under-test (DUT), while the other acts simply as a trigger to indicate when a correlated photon can be expected at the DUT. For the trigger channel (A in this case) a short range of wavelengths, defined by a narrow-bandwidth interference filter, and an iris is used (see Fig. 1), while for the second channel (B=DUT) the spectral bandpass and collection iris are larger, ensuring that all photons correlated to those arriving at A fall on B. This is crucial to a simple understanding of the ultimate accuracy of the technique. Consequently the second relation in Eq. (4) is rewritten as

$$\eta_{DUT} = \frac{1}{T_B} \frac{N_C}{N_{trigger}}, \qquad (5)$$

where T_B is the transmittance of the portion of the optical path, B, that is not included in DUT itself.

We report on the absolute calibration of the same APD operating as a single photon counter (referred to as DUT-NIST) performed independently in two laboratories, the National Institute of Standards and Technology (NIST) and the Istituto Elettrotecnico Nazionale (IEN). Similar experimental setups have been used, and a procedure of measurement is pro-

posed to determine empirically the accuracy limits of the technique.

The aim here is to demonstrate by comparison the inherent absoluteness of the measurements and their independence of the particular PDC generation and trigger detection setups and to highlight the systematic effects limiting the uncertainty. Once this is done a measurement protocol can be developed to help move this technique from the realm of simple demonstrations into the world of metrology.

In addition to the above the same setup used for comparison at IEN was also used to calibrate a fiber-coupled APD (DUT-IEN) to demonstrate the generality of the procedure. Uncertainty evaluations are shown for both DUT calibrations and experimental setups, and differences and similarities are presented.

2. Experimental Setup for Laboratory Comparison

The arrangements for the quantum efficiency measurements at NIST and IEN were generally similar (Fig. 1). A linearly polarized argon-ion laser operating at 351.1 nm was used to pump a nonlinear crystal, NLC. A half-wave plate ($\lambda/2$) was used to allow rotation of the polarization of the pump beam. This enabled the PDC process to be turned off, because the phase-matching condition permits only one pump polarization to be downconverted. This was used to determine scatter and dark count rates.

At IEN the nonlinear crystal used was a 5-mm-long $LiIO_3$ crystal, housed in a sealed holder filled with dry nitrogen. The crystal was cut and tilted for phase matching at 51.7° and was mounted to allow rotation about the normal to the crystal surface. The output window of the crystal housing and the output surface of the crystal produced a total reflective loss of $(4.1 \pm 0.1)\%$, as measured at 633 nm. Standard uncertainties ($k = 1$) are used throughout this paper.[10] This level of reflectance is lower than expected for bare surfaces but higher than expected for typical antireflection-coated surfaces. This occurred because the output surfaces were antireflection coated but not optimized for the 633-nm light of our measurements. The crystal presented negligible absorption of ~0.2% over the 5-mm length at 633 nm.

At NIST a bare KDP crystal 5 mm long was used. The bare KDP crystal presented a 4.1% reflectance per surface at normal incidence. The crystal absorption was found to be negligible (<0.05%). Similar downconversion geometries were used in both laboratories with the downconverted light of interest (633 and 789 nm) emitted between 3° and 5°.

Both the trigger and the DUT detectors were APD photon-counting modules equipped with active quenching circuits and built-in discriminators. These modules produce nearly square pulses 8 ns wide and 2 V in amplitude. The distances from the detectors to the source were chosen in both laboratories to be 1 m for the DUT and 2 m for the trigger. Both detectors were mounted on translation-tilt stages.

The detector calibrated in the comparison (DUT-NIST) was a single-photon APD with a sensitive area 500 μm in diameter with a built-in active quenching circuit (EG&G SPCM-AQ-231).[11] The DUT and the optics (L_{DUT}, F_{DUT}) were from NIST: L_{DUT} was a collection lens with a 25-mm focal length, mounted 25 mm from the DUT sensitive area; F_{DUT} was an interference filter peaking at 633 nm with a 10-nm FWHM. I_{DUT} was an iris with a variable diameter from 1.5 to 10 mm. For the comparison the DUT was mounted with its collection lens, spectral filter, and collection iris as a unit that could be translated horizontally and vertically as well as tilted. The NIST setup used a trigger detector unit identical to the DUT-NIST.

At IEN the trigger detector was similar but not identical to the DUT: It was an EG&G Model SPCM-AQ-152-FC with a sensitive area of ~0.025 mm^2 (180 μm in diameter) and dark counts below 50 counts/s. This detector was coupled to a small length (1 m) of multimode optical fiber. The PDC signal was coupled into the fiber with a 20× microscope objective ($L_{trigger}$). The trigger beam was spectrally limited by an interference filter peaked at 789 nm and with a 3-nm FWHM.

Coincidences and single counts were measured in both experiments by nearly identical electronics. The output signal from the trigger detector was sent to the start input of the time-to-amplitude-converter (TAC) circuit. The DUT output was delayed and sent to the stop input of the TAC. The TAC output was sent to a multichannel analyzer that recorded histograms of interarrival times of the DUT and trigger events. Correlated photon pairs are seen in the histogram as a peak whose width is due to the combined time jitter of the detectors and the electronics. This peak is on top of a flat background resulting from uncorrelated output pulses of detectors. True coincidences are found by counting the events within a fixed time window around this peak and subtracting the flat background level within this same time window (referred to as accidental coincidences). The coincidence window must be set wide enough to contain all the true coincidences: To achieve uncertainties much below 1% it must be set many times the FWHM of the coincidence peak[12] owing to the long tails of the peak. At IEN the window was (3.88 ± 0.01) ns, while the peak FWHM was 0.54 ns.

Correction for accidental counts must be measured or calculated. At NIST two windows were set on the multichannel analyzer, one to record the total coincidences and a larger one away from the peak to determine the rate of accidental counts. At IEN accidental counts were calculated. We have proved the theoretical formula for the accidental coincidence counts in Ref. 13.

To show the versatility of the procedure, we also calibrated a fiber-coupled APD (DUT-IEN) identical to the trigger detector of the IEN comparison setup. DUT-IEN is a package consisting of an interference filter centered at 632.8 nm with a bandpass FWHM of 10 nm, microscope objectives, and multimode fiber as

described above. Attention was paid to the fiber-coupling stability and alignment of both detectors. Losses due to the fiber and the coupling lenses were not determined individually because we considered them to be part of the DUT detector.

3. Measurement Procedure

To obtain high reproducibility, allowing comparable measurement results from the two laboratories, we attempted to establish an optimal and robust procedure. High-accuracy measurements can be achieved if the system is designed to maximize the collection of all photons correlated to those seen by the trigger detector. Collection system losses are of two types: conventional transmittance losses due to reflectance and absorptance of the optical components in the DUT optical path or geometric ones, such as those due to limiting irises and detector misalignment.

The first loss type can be handled straightforwardly; the transmittance of optical components can be directly measured with high accuracy and/or the losses can be calculated. For the IEN experiment the losses due to the crystal were measured with a He–Ne laser: We accounted for reflection losses on the output window and the absorption loss inside the crystal. Assuming that PDC-generated light traverses on average half of the crystal length, we obtained a crystal transmittance of 0.959 ± 0.002. Conventional transmittance losses due to the collection lens and interference filter were the same in both experimental setups, because the lens–filter–detector package was calibrated as a whole.

More difficult to analyze were the geometric losses. They can be divided into two types. First and most trivially the DUT may be misaligned with the center of path of photons correlated to those seen by the trigger. Second, losses in the DUT collection path can be due to the spread of emission positions and directions of photons correlated to those seen by the trigger detector. The causes of this spreading, which have been treated elsewhere,[14] are due to such things as the finite diameter of the pump beam and the finite length of the nonlinear crystal. The finite spectral bandwidth of light seen by the DUT that is correlated to the trigger is determined by the spectral band of the light seen by the trigger through the energy conservation rule. Thus it is important that any frequency-selective element in the DUT optical path is broad enough to include all correlated frequencies. The finite spread of frequencies corresponds to a finite spread of angles, so that the trigger collection angle also puts constraints on the geometric collection of the DUT.

A. Detector Alignment
The detector-alignment procedure is as follows: First, the trigger detector position is translated radially across the cone of downconverted light to maximize the single-photon signal. This centers the detector on the central wavelength of the spectral filter. The DUT must then be centered radially and tangentially along the downconverted light cone on
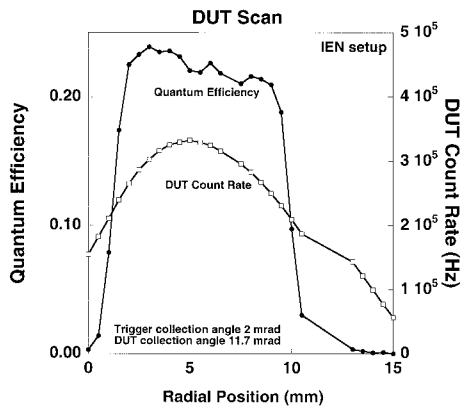
Fig. 2. DUT-NIST quantum efficiency as the DUT-NIST is scanned radially across the cone of downconversion light in the IEN setup (●): The value of quantum efficiency is corrected for transmittance of the crystal, dark counts, and accidental counts. □, the DUT count rate.

the light correlated to the trigger. Because the detector package includes a collection lens, centering the DUT package on the correlated beam involves iterative optimization of its translational position and its angular orientation. This procedure consists of stopping down the collection lens iris before translationally maximizing the correlated signal. Then the detector/lens package is tilted about the lens po-

sition, allowing the detector to be positioned at the focused spot of light. These two steps are repeated until no further gains are seen.

A check of the trigger position must be performed by translational scan to verify that the maximum correlated signal occurs at the maximum of the single trigger counts. Thus, by successive iterative scans of both detectors, we achieve maximum overlap of the two detectors on the correlated pairs. Figure 2 shows the final results of the alignment procedure with I_{DUT} fully open (11.7-mrad collection angle) and I_{trigger} with a 4-mm diameter (2-mrad collection angle) for the IEN setup. The procedure described above was used to calibrate DUT-IEN. The resulting DUT and trigger translational scans are shown in Fig. 3 (I_{DUT} fully open with a collection angle of 9.4 mrad limited by the objective aperture). In this case the procedure was used to optimize the fiber coupling to correlated photons. It is clear from Fig. 3 that the radial position of DUT is more critical than the trigger position, which presents a larger flat region at the maximum quantum efficiency level. This is mainly because of the narrower DUT collection angle with respect to Fig. 2. Figure 4 shows the quantum efficiency, and DUT counts for a radial scan of DUT-IEN position for two different tilt angles of the package consisting of the filter and fiber-coupling optical system in the IEN setup. Note that, while the tilt has
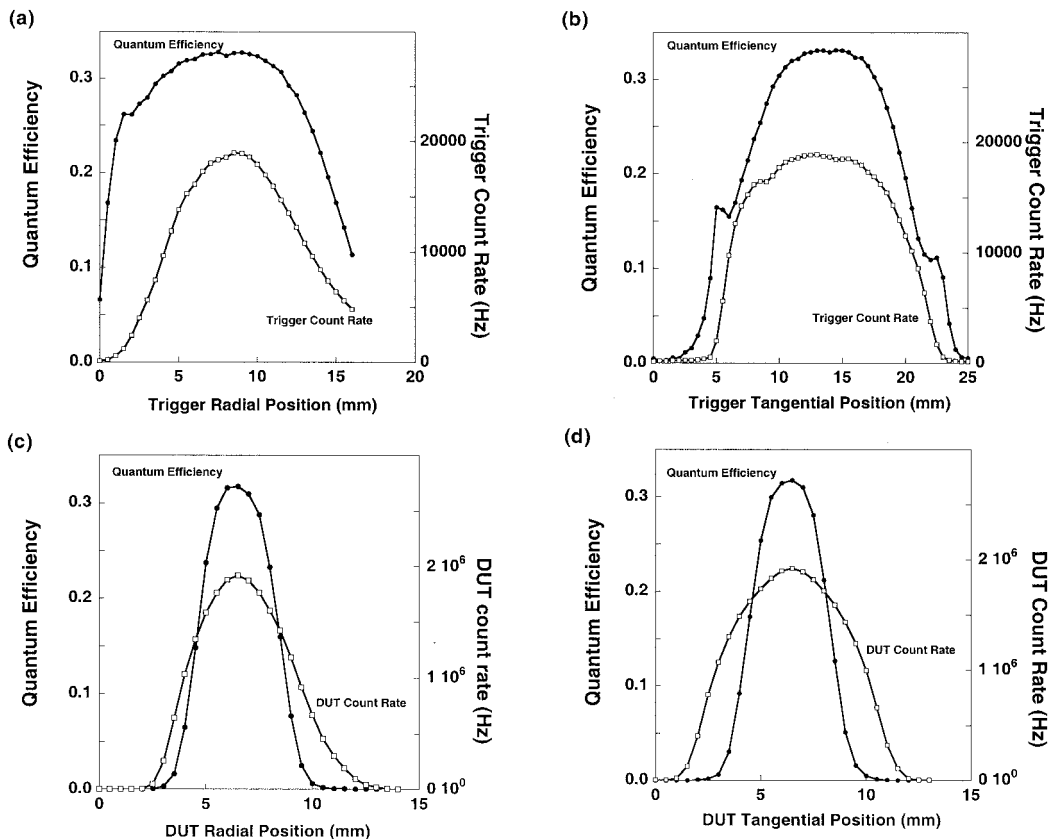
Fig. 3. Measurement of DUT-IEN performed at IEN as a trigger detector is moved (a) radially and (b) tangentially to the cone of downconverted light, while (c) and (d) show the same results except that the DUT is moved instead: ●, quantum efficiency, □, trigger count rate in (a) and (b) and the DUT count rate in (c) and (d).

DUT Scan
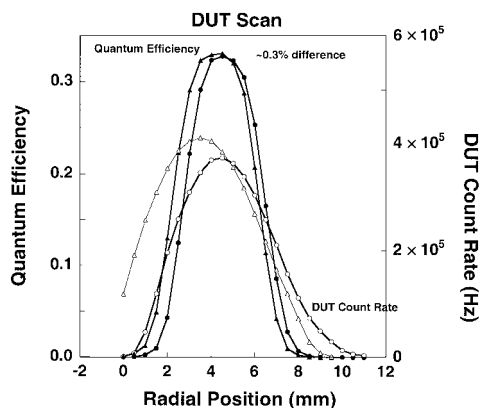
Fig. 4. Quantum efficiency (▲, ●) and DUT counts (△, ○) values for two tilting positions of the DUT-IEN detector as it is scanned radially.

a significant effect on the DUT singles count rate due to shifts in the filter transmittance passband, it has very small effect on the resulting quantum efficiency determination because the DUT filter passband exceeds the spectral range of the photons correlated to the trigger. The quantum efficiency values reported are corrected for the following effects present in the IEN experimental setup: dark counts, accidental coincidence counts, TAC dead time, and optical losses in the crystal.[15]

B. Collection-Angle Verification

A further check of the alignment of the DUT and trigger was obtained by scanning both detectors versus collection angles to optimize the correlated signal. Figure 5(a) shows a scan of quantum efficiency versus collection angle for the DUT-NIST in the NIST setup. The apparent quantum efficiency of the DUT is seen to level off to better than ±0.25% for a DUT collection angle greater than 6 mrad. This is consistent with a trigger detector collection angle of 2.2 mrad. A complementary measurement [Fig. 5(b)] was made by fixing the DUT collection angle at 6.5 mrad [the start of the level region of Fig. 5(a)] and scanning the trigger collection angle. A drop in apparent quantum efficiency is seen as the trigger collection angle exceeds 2.2 mrad, causing the angular range of the correlated photons to exceed the collection range of the DUT.

The same measurement was performed at IEN. Figure 6 shows the quantum efficiency versus the DUT collection angle. The quantum efficiency is seen to level out at a collection angle of ~4.7 mrad for a trigger collection angle of 2 mrad. The small downward slope of quantum efficiency with a higher collection angle is due to an increasing detector dead time as the DUT singles counts continue to rise nearly linearly with the collection angle. This level of variation (±0.8%) is higher then those seen at NIST. This difference is likely due to a higher DUT deadtime and higher DUT count rates with respect to the trigger at IEN: In fact the maximum DUT count rate was 250 kHz, while the trigger was 2.2 kHz.

(a)

(b)
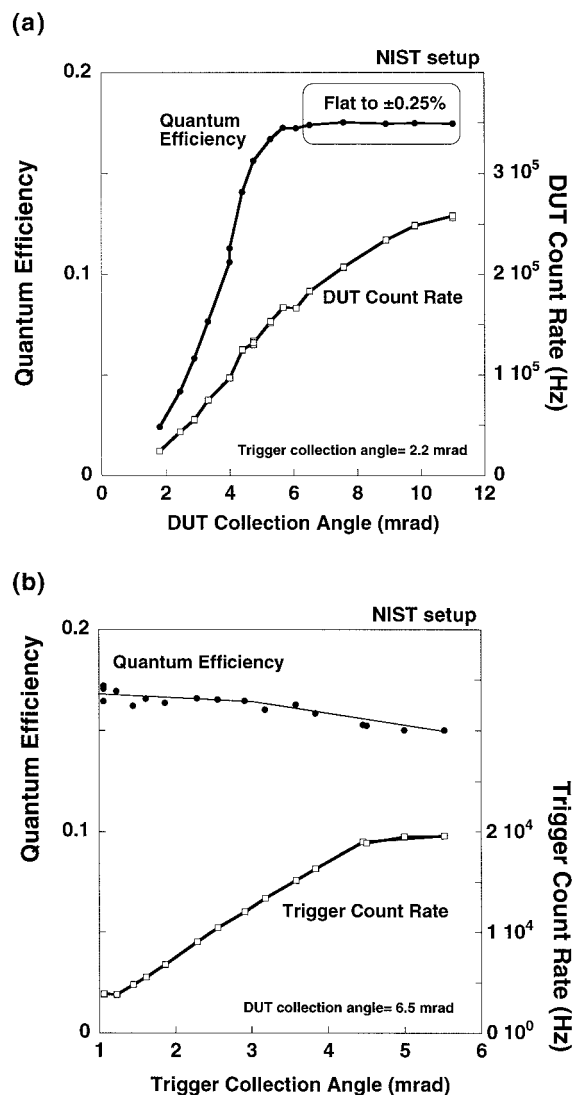
Fig. 5. (a) Apparent quantum efficiency of the DUT-NIST and its singles count rate shown as the DUT collection lens iris is varied with the trigger detector collection angle of 2.2 mrad. (b) Apparent quantum efficiency of the DUT and trigger singled count rate shown as the trigger collection lens iris is varied with the DUT detector collection angle fixed at 6.5 mrad. The quantum efficiency is not corrected for crystal losses.

C. Determination of the True Trigger Rate

The simple formula given in Eq. (5) has to be modified to account for the presence of unwanted counts. In fact each detector is affected by background counts, resulting from stray light unrelated to the downconversion pairs and electronic noise (dark counts). The measurement of dark counts plus stray light is made with a wave plate in the pump beam. This wave plate can be used to rotate the polarization of the pump beam by 90°, which effectively turns off the creation of photon pairs, because the phase-matching constraints allow only one polarization orientation of the pump beam to produce downconverted light. The advantage of this scheme is that, while the production of photon pairs is stopped, all other scattered
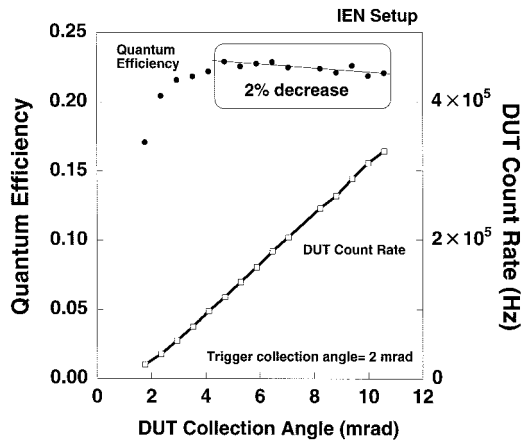
Fig. 6. Quantum efficiency of the DUT-NIST measured at IEN, ●, and its singles count rate, □, shown as the DUT collection lens iris is varied with the trigger detector collection angle of 2 mrad. Quantum efficiency is not corrected for crystal losses. The spot on the detector surface to be measured was not reproducibly chosen, so the difference in quantum efficiency maximums in this figure and that shown in Figs. 5(a) and 5(b) is most likely due to variations of quantum efficiency over the detector surface. As we see in Fig. 10 this variation can be large.

light remains the same, allowing an excellent determination of the total scattered-light level.

Figure 7(a) shows the trigger count rate as the pump polarization was scanned (in the NIST setup). The minimum level, an indication of the scattered-light count rate, was found to be $(0.020 \pm 0.006)\%$ of the maximum. A similar measurement was performed at IEN, yielding a minimum trigger rate of $(0.003 \pm 0.080)\%$ [see Fig. 7(b)].

Care must be taken with this technique to avoid overestimating the scatter level. If the pump beam is not pure linear polarization at the wave plate, the downconversion process will not be completely turned off at the minimum point of the curve and the apparent scattered/dark level will be too high. This was checked by also monitoring the coincidence rate at the minimum point of the curves in Fig. 7. With the NIST setup we found that the minimum coincidence rate was $(0.03 \pm 0.01)\%$ of the maximum rate, while at IEN it was $(0.005 \pm 0.003)\%$, both acceptably low levels.

D. Quantum Efficiency Stability

A stability test was performed at NIST and IEN. Figure 8(a) shows the NIST quantum efficiency measurements exhibiting a mean drift of $\approx 0.07\%$ and a 0.3% repeatability at one point on the detector surface over a 7-h period. That the quantum efficiency determination remained nearly constant, even as the trigger rate drifted by 4%, highlights the overall robustness of this primary standard method: The quantum efficiency is independent of trigger count rates, as expected.

The same measurements were performed at IEN on a fiber-coupled APD. Figure 8(b) shows the tem-
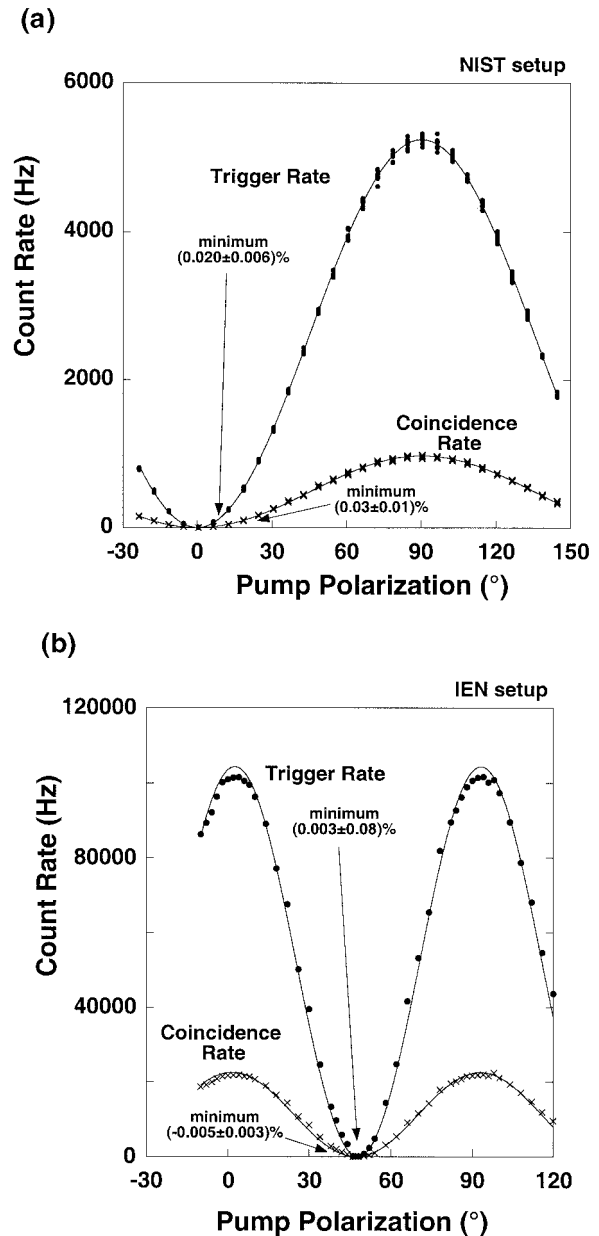
Fig. 7. (a) Trigger, ●, and coincidence, ×, count rates shown as the pump polarization is rotated (in the NIST setup). The minimum trigger rate is 0.02% of the maximum signal (after subtracting for detector dark counts), while the coincidence rate falls to a level of 0.03%. (b) The same measurement performed at IEN yielding similar results.

poral variation of the trigger counts and the quantum efficiency. The observed trigger drift was 0.7% over 1.5 h, while the quantum efficiency drift was much less. We used the 0.3% fluctuations over 1.5 h as an estimate of the standard uncertainty ($k = 1$) of quantum efficiency measurements. As with the NIST measurements this empirically supports the claim that measurement of quantum efficiency by the correlated photon method is independent of the trigger detector quantum efficiency or variations of its quantum efficiency.

(a)

(b)
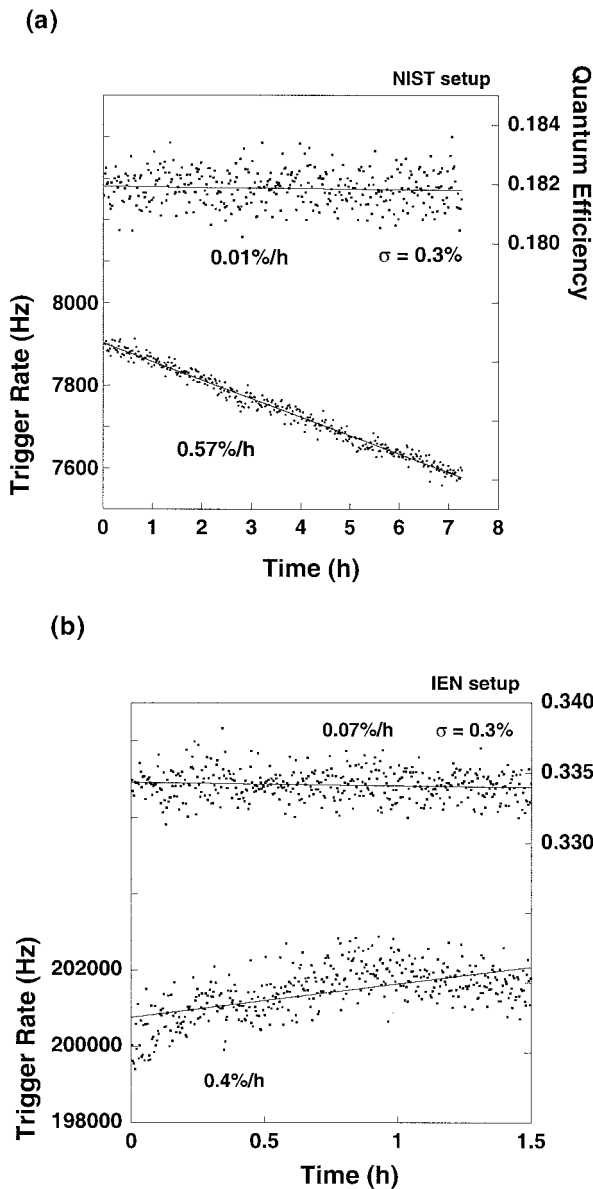
Fig. 8. (a) Stability of the quantum efficiency at one point on the detector surface as the trigger count rate falls, measured at NIST. This highlights the robustness of the quantum efficiency determination. The relative standard deviation of the quantum efficiency measurements was 0.3%. (b) Short-term measurement of DUT-IEN made at IEN. Here the 0.3% relative fluctuations are of the order of the estimated uncertainty, meaning that trigger-count drifts have little effect on the measurement.

E. Spatial Uniformity of DUT-NIST

At both IEN and NIST the spatial uniformity of the DUT-NIST sensitive area was determined by tilting the detector–filter–lens as a unit. Because the lens was near the center of the tilt motion, while the APD was farther away, a tilt of the entire unit effectively scanned the detector relative to the focused spot of correlated light at the detector surface. Manual scans of the detector showed large quantum efficiency variations with extremes of 0.194–0.242 (see Fig. 9 for measurements made with the IEN setup). Note
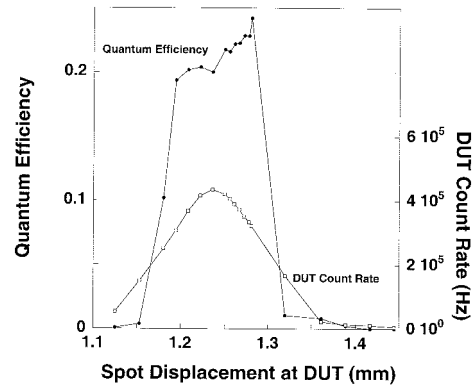
Fig. 9. Variation of quantum efficiency, ●, and DUT-NIST count rate, □, as the package filter–lens–detector is tilted (measured in the IEN setup).

that these variations are in stark contrast to the low variations that can be achieved with high-performance analog Si detectors.[16] The detector was not specifically scanned through its center, so the observed detector width is likely to be smaller than its diameter. Note that Fig. 2 shows a similar shape because translation of the DUT package also has the effect of scanning the correlated light spot across the detector. To investigate this variation in detail, an automated system was subsequently built at NIST to take complete raster scans of the detector efficiency. For this scan the detector was separated from the lens and the filter mount and moved separately, eliminating the possibility of any unwanted optical effects from tilting optics. Figure 10 shows the result at NIST: The maximum quantum efficiency is 40% larger than the minimum value. The edges indicate that the full width of the correlated spot is no larger than 50 μm. The large variation seen here is consistent with the results of the simple manual tilting obtained at IEN (Fig. 9) and that, although we were not able to make a rigorous comparison, we can clearly see qualitative agreement and some quantitative agreement between the measurements in the two laboratories. For more rigorous interlaboratory comparisons a detector with better spatial uniformity would be clearly desirable.

4. Uncertainty Evaluation

Because of the poor spatial response uniformity of DUT, the measurements in the two laboratories could not be directly compared to provide an independent test of the measurements. As a result we have instead used two methods to quantify the measurement uncertainty. One method relies on statistical evaluation, while the other is determined by experimental means. The two methods produce consistent results.

The statistical uncertainty is deduced by applying the uncertainty propagation law to the model of measurement as described in Ref. 15, calculated according to Ref. 17. In Table 1 we report the relative uncertainty budget of the quantum efficiency

Raw Counts (rel.)

0.5 mm

0.5 mm

Quantum Efficiency

0.24
0.22
0.20
0.18

0.5 mm

0.5 mm
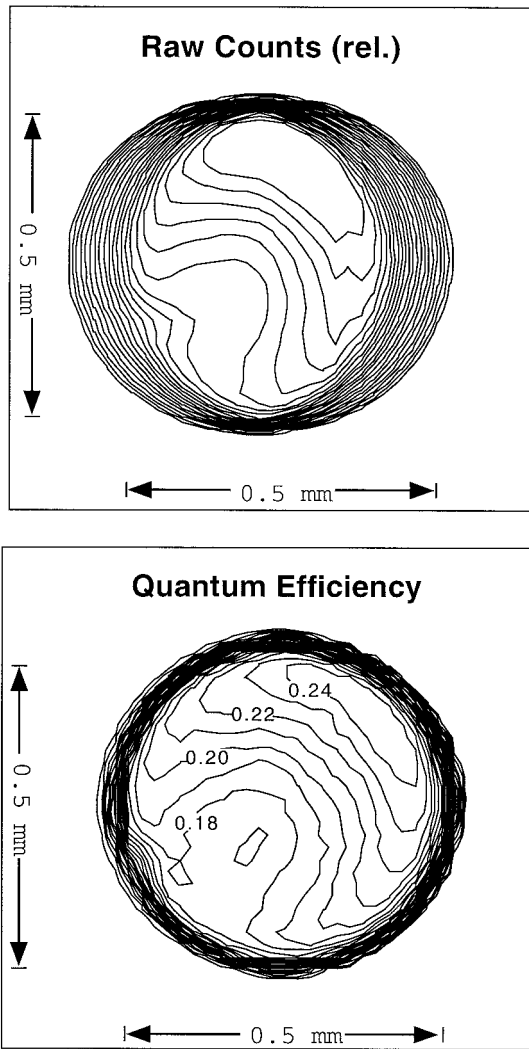
Fig. 10. Spatial maps of (a) quantum efficiency and (b) raw counts at 633 nm (these efficiencies include crystal transmittance losses) as DUT-NIST was scanned across the downconverted light beam at NIST.

measurements made with the IEN setup of the DUT-NIST and DUT-IEN detectors (for a single location on the detector active area) at comparable count rates. Here the total uncertainty is calculated, taking account of the statistical correlation coefficient,

$$\rho_{N_{\text{trigger}}, N_C} = \frac{(\langle N_C N_{\text{trigger}} \rangle - \langle N_C \rangle \langle N_{\text{trigger}} \rangle)}{[u^2(N_C) u^2(N_{\text{trigger}})]^{1/2}}, \quad (6)$$

that contributes to the reduction of the total uncertainty, where $u^2(x) = <x^2> - <x>^2$ is the variance of a generic variable x. Equation (6) means that fluctuations of the trigger and coincidence rates are correlated as expected, because fewer (or extra) counts in the trigger channel have a significant probability of yielding fewer (or extra) counts in the coincidence channel. Thus the total uncertainty can be smaller than the largest single component (as seen in the second column of Table 1).

Table 1. Uncertainty Budget for Calibrations of DUT-NIST and DUT-IEN Made in an IEN Setup[a]

Uncertainty Component	Relative Uncertainty Contribution ($k = 1$) (%)	
	DUT-IEN	DUT-NIST
Trigger counts	0.33	1.13
Dark counts	0.02	0.25
Coincidence counts	0.45	2.01
Optical losses	0.46	0.46
DUT counts	<0.01	<0.01
Coincidence window	<0.01	<0.01
Residual dead time	0.02	0.02
Total uncertainty		
Statistical correlations excluded	0.72	2.36
Statistical correlations included	0.56	1.87

[a]The relative uncertainty is evaluated with a Gaussian propagation model that accounts for statistical correlation as described in Ref. 15.

Note: There is a statistical correlation between trigger and coincidence counts results as a negative contribution to the total uncertainty by Eq. (6). This correlation was empirically evaluated as 0.46 and 0.68 for DUT-NIST and DUT-IEN, respectively. The total uncertainty excluding statistical correlations (i.e., simple quadrature sum) is given for comparison on the next to the last row.

Note that in the case of the DUT-NIST calibration at IEN the noise associated with the trigger counts, due to a somewhat unstable fiber coupling, was greater than for the case of DUT-IEN calibration, resulting in a greater measurement uncertainty in the first case.

An alternative method for evaluating uncertainty is shown in Table 2. The uncertainty budget is given for quantum efficiency measurements of the DUT-NIST in the IEN and NIST setups, where the final uncertainties are deduced by experimental means, by using, for example, the variations as seen in Figs. 5, 6, and 8 and the results in Fig. 7. Note that the uncertainty associated with DUT-NIST in the IEN setup turns out to be lower if evaluated by

Table 2. Uncertainty Budget for Calibrations of DUT-NIST Performed in the NIST and IEN Setups

Uncertainty Component	Relative Uncertainty contribution ($k = 1$) (%)	
	NIST Setup	IEN Setup
DUT iris test result	0.25	0.80
Trigger noise	0.08	1.70
Stability test result	0.30	1.11
Optical losses	<0.1	0.80
Pump polarization purity test result	0.007	0.35
Total uncertainty	0.40	2.35
Total DUT spatial nonuniformity	40	25

Note: Here the uncertainty was determined empirically according to the procedure described in this research. The last row shows the measured spatial variation of the DUT-NIST. This level of variation clearly limits how well measurements made in the different setups can be compared.

the statistical method rather than by the empirical one (1.87% versus 2.35%). This last method may overestimate uncertainty because it does not include possible statistical correlations.

5. Conclusions

We have shown the results of calibrating an avalanche photodiode from NIST in setups at IEN and NIST by using a correlated photon technique. A procedure has been sketched for a interlaboratory comparison to minimize and empirically quantify systematic effects. The results show qualitative consistency between the two laboratories. At this time the overall uncertainty is limited by the spatial uniformity of the detector under test rather than the measurement method itself. A measurement of this nonuniformity has been given.

We performed a further calibration of an IEN fiber-coupled avalanche photodiode with the same experimental setup, following the procedure established, yielding an improved uncertainty relative to a previous calibration done at IEN. We have studied contributions to the uncertainty of this kind of measurement. We have established that pump laser instability contributes little to the final uncertainty, highlighting the inherent absolute nature of the measurement method. The procedure is currently under test, and improvement in both laboratories and a measurement protocol is under development.

References and Notes

1. S. Castelletto, A. Godone, C. Novero, and M. L. Rastello, "Biphoton fields for quantum-efficiency measurements," Metrologia **32,** 501–503 (1996).
2. D. C. Burnham and D. L. Weinberg, "Observation of simultaneity in parametric production of optical photon pairs," Phys. Rev. Lett. **25,** 84–87 (1970).
3. D. N. Klyshko, *Photons and Nonlinear Optics* (Gordon and Breach Science Publishers, New York, 1988).
4. V. M. Ginzburg, N. G. Keratishvili, Y. L. Korzhenevich, G. V. Lunev, and A. N. Penin, "Absolute measurement of quantum efficiency based on parametric downconversion effect," Metrologia **30,** 367–368 (1993).
5. P. G. Kwiat, A. M. Steinberg, R. Y. Chiao, P. H. Eberhard, and M. D. Petroff, "Absolute efficiency and time-response measurement of single-photon detectors," Appl. Opt. **33,** 1844–1853 (1994).
6. A. L. Migdall, R. U. Datla, A. Sergienko, J. S. Orszak, and Y. H. Shih, "Absolute detector quantum-efficiency measurements using correlated photons," Metrologia **32,** 479–483 (1996).
7. G. Brida, S. Castelletto, C. Novero, and M. L. Rastello, "Measurement of quantum efficiency of photodetectors by parametric fluorescence," Metrologia **35,** 397–401 (1998).
8. A. N. Penin and A. V. Sergienko, "Absolute standardless calibration of photodetectors based on quantum two-photon fields," Appl. Opt. **30,** 3582–3588 (1991).
9. J. G. Rarity, K. D. Ridley, and P. R. Tapster, "Absolute measurement of detector quantum efficiency using parametric downconversion," Appl. Opt. **26,** 4616–4619 (1987).
10. B. N. Taylor and C. E. Kuyatt, "Guidelines for evaluating and expressing the uncertainty of NIST measurement results," NIST (Natl. Inst. Stand. Technol.) Tech. Note 1297 (1994).
11. Certain trade names and company products are mentioned in the text or identified in an illustration in order to specify adequately the experimental procedure and equipment used. In no case does such identification imply recommendation or endorsement by the National Institute of Standards and Technology or by the Istituto Elettrotecnico Nazionale, nor does it imply that the products are necessarily the best available for the purpose.
12. A. Migdall, "Absolute quantum efficiency measurements using correlated photons: toward a measurement protocol," IEEE Trans. Instrum. Meas. **50,** 478–481 (2001).
13. I. P. Degiovanni, "Application of nonlinear optical effects to quantum radiometry," Ph.D. Polytechnico of Turin, Turin, Italy, in preparation.
14. N. Boeuf, D. Branning, I. Chaperot, E. Dauler, S. Guerin, G. Jaeger, A. Muller, and A. Migdall, "Calculating characteristics of noncollinear phase-matching in uniaxial and biaxial crystals," Opt. Eng. **39,** 1016–1024 (2000).
15. G. Brida, S. Castelletto, I. P. Degiovanni, C. Novero, and M. L. Rastello, "Quantum efficiency and dead time measurement of single-photon photodiodes: a comparison between two techniques," Metrologia **37,** 625–628 (2000).
16. A. R. Schaefer and J. Geist, "Spatial uniformity of quantum efficiency of a silicon photovoltaic detector," Appl. Opt. **18,** 1933–1936 (1979).
17. G. Sauter, "Determination of measurement uncertainty in photometry," to be published.